

Calculation of neoclassical toroidal viscosity with a particle simulation in the tokamak magnetic braking experiments

This content has been downloaded from IOPscience. Please scroll down to see the full text.

2014 Nucl. Fusion 54 073014

(<http://iopscience.iop.org/0029-5515/54/7/073014>)

View [the table of contents for this issue](#), or go to the [journal homepage](#) for more

Download details:

IP Address: 198.125.229.230

This content was downloaded on 28/04/2014 at 17:01

Please note that [terms and conditions apply](#).

Calculation of neoclassical toroidal viscosity with a particle simulation in the tokamak magnetic braking experiments

K. Kim^{1,a}, J.-K. Park¹, A.H. Boozer², J.E. Menard¹,
S.P. Gerhardt¹, N.C. Logan¹, Z.R. Wang¹, G.J. Kramer¹,
K.H. Burrell³ and A.M. Garofalo³

¹ Princeton Plasma Physics Laboratory, Princeton, NJ 08543, USA

² Department of Applied Physics and Applied Mathematics, Columbia University, New York, NY 10027, USA

³ General Atomics, San Diego, CA 92186, USA

E-mail: kkim@pppl.gov

Received 22 October 2013, revised 17 March 2014

Accepted for publication 17 March 2014

Published 24 April 2014

Abstract

Accurate calculation of perturbed distribution function δf and perturbed magnetic field δB is essential to achieve prediction of non-ambipolar transport and neoclassical toroidal viscosity (NTV) in perturbed tokamaks. This paper reports a study of the NTV with a δf particle code (POCA) and improved understanding of magnetic braking in tokamak experiments. POCA calculates the NTV by computing δf with guiding-centre orbit motion and using δB from the ideal perturbed equilibrium code (IPEC). Theories of NTV for magnetic field resonance, collisionality dependency, and toroidal mode coupling are tested in the simple configurations using the particle simulations. The POCA simulations are also compared with experimental estimations for NTV, which are measured from angular momentum balance (DIII-D) and toroidal rotational damping rate (NSTX). The calculation shows reasonable agreement in total NTV torque for the DIII-D discharge with weak rotational resonances in the $\nu_{-}\sqrt{\nu}$ regime. In NSTX discharges where the bounce-harmonic resonances dominantly appear, the POCA simulation gives total NTV torques comparable to the measurements, however large discrepancies are found in the detailed damping and NTV profiles. It is discussed that a self-consistent calculation of δB using general perturbed equilibria is eventually necessary since a non-ideal plasma response can change the perturbed field and thereby the NTV torque.

Keywords: tokamak, NTV, magnetic braking, 3D field, drift-kinetic particle simulation

(Some figures may appear in colour only in the online journal)

1. Introduction

Magnetic perturbations in tokamaks, induced by intrinsic error fields or externally applied non-axisymmetric fields, distort particle orbits through deformed or broken flux surfaces and can fundamentally change neoclassical transport [1–3]. In particular, modification in toroidal momentum transport and toroidal rotation can be pronounced apparently due to the toroidal symmetry breaking in the magnetic field, as often called magnetic braking of toroidal rotation via neoclassical toroidal viscosity (NTV) [4–6]. Since even a magnetic perturbation as small as $|\delta B/B| \sim 10^{-4}$ can substantially change toroidal rotation and thus various plasma instabilities [7–9], it is not only essential to understand physics but also to develop a highly precise tool for prediction of magnetic braking and NTV.

One of key components in NTV description is the calculations of δf , the perturbed distribution function, on non-axisymmetric magnetic field perturbations δB . Substantial progress has been made in physics understanding by analytic δf treatments [10–15]. However, in order to achieve accuracy required for NTV prediction in practice, numerical calculations are necessary to avoid various approximations in analytic theories such as large aspect-ratio expansion, bounce-averaging of trapped particles, zero-banana-orbit width, regime separation, or simplified collision operators. POCA (Particle Orbit Code for Anisotropic pressures) has been developed for this purpose [16], and to provide improved NTV predictability by following exact guiding-centre orbit motions of particles and precisely calculating δf and NTV. In addition to actual applications to magnetic experiments, POCA has also been actively used to verify several fundamental aspects that were predicted in NTV theories.

^a Author to whom any correspondence should be addressed

In this paper, the applications of the particle simulation code, POCA to calculation of NTV in magnetic braking experiments for DIII-D and NSTX are presented by computing δf with the guiding-centre orbit motion and using δB from the ideal perturbed equilibrium code, IPEC. Section 2 describes the methods to calculate δf and NTV in POCA simulations. Numerical tests of NTV physics, such as collisional dependencies in the presence of precession, and mode coupling or decoupling, are presented in section 3. A technique for reconstructing δB including ideal plasma responses for experimental applications is explained in section 4. Then POCA applications to actual magnetic braking experiments in DIII-D and NSTX are presented in section 5, where the NTV torques, obtained from global angular momentum balance in DIII-D and estimated from rotational damping rate in NSTX, are compared with the POCA simulation and the combined NTV theory. Issues for improving the NTV prediction are discussed in section 6, and the concluding remarks are given in section 7.

2. Guiding-centre particle simulation for calculation of δf and NTV

A guiding-centre orbit code, POCA solves the Fokker–Planck equation with a δf Monte Carlo method to obtain the perturbed distribution function δf [16, 17]. The Fokker–Planck equation is written as

$$\frac{d \ln f_M}{dt} + \frac{d \hat{f}}{dt} = C_m, \quad (1)$$

where the distribution function f is approximated to $f \approx f_M(1 + \hat{f})$ with the local Maxwellian f_M , and $C_m \equiv C/f$ with the pitch-angle scattering collision operator C modified to conserve the toroidal momentum [17]. The reduced Fokker–Planck equation can be rewritten as

$$\frac{d \hat{f}}{dt} = -\vec{v} \cdot \vec{\nabla} \psi \frac{\partial \ln f_M}{\partial \psi} + C_m, \quad (2)$$

then \hat{f} is obtained by

$$\Delta \hat{f} = - \left[\frac{1}{N} \frac{\partial N}{\partial \psi} + \left(\frac{3}{2} - \frac{E}{T} \right) \frac{1}{T} \frac{\partial T}{\partial \psi} \right] \Delta \psi + 2\nu \frac{u}{v} \lambda \Delta t - \frac{e}{T} \frac{d\Phi}{d\psi} \Delta \psi, \quad (3)$$

where ν is the collision frequency, u is the parallel flow velocity, λ is the pitch-angle, and Φ is the electric potential. The first term in the right hand side of equation (3) represents the δf driven by particle drift motions, and the second term is the momentum correction term to preserve the toroidal momentum conservation. The last term represents the electric potential effect, which is directly related to the toroidal rotation and $\vec{E} \times \vec{B}$ precession by $E_r = -d\Phi/dr$.

The particle trajectories in guiding-centre motion between collisions are then calculated by the Hamiltonian orbit equations on Boozer coordinates [18]. An example of the guiding-centre drift motion in an axisymmetric NSTX plasma is illustrated in figure 1, reflecting a typical feature of the magnetic field line structures in NSTX. As presented in [16], the distortion of this guiding-centre motion by non-axisymmetric perturbation can lead to rapid radial transport, and thus to radial current and toroidal torque with NTV.

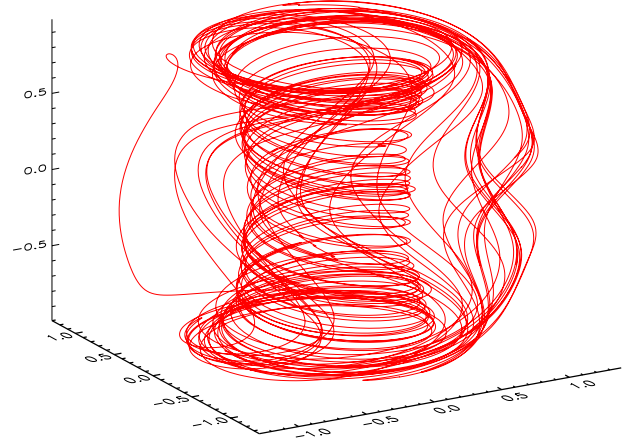


Figure 1. Three-dimensional (3D) trajectory of a single guiding-centre orbit motion in an axisymmetric NSTX plasma, calculated by POCA. Collisions were neglected here.

In POCA simulations, NTV torque is obtained by evaluating perturbed anisotropic pressure [19, 20]. In Boozer coordinates,

$$\tau_\varphi \equiv \langle e_\varphi \cdot \nabla \cdot \mathbf{P} \rangle = \left\langle \frac{\delta P}{B} \frac{\partial B}{\partial \varphi} \right\rangle, \quad (4)$$

where $e_\varphi = \partial \mathbf{x} / \partial \varphi$, δP is the perturbed pressure defined by $\delta P = \int d^3 v (M v_\parallel^2 + M v_\perp^2 / 2) \delta f$, and the brackets denote the flux surface average. These POCA calculations for NTV have been successfully tested with semi-analytic methods in zero precession limits, and have also numerically demonstrated several key aspects in NTV physics, such as δB^2 dependence, phase-mixing by toroidal precession, and rotational resonances such as bounce-harmonic resonances, as presented in [16, 21]. The further numerical tests on other key aspects, such as field resonance, the collisionality dependence in finite toroidal precession, and mode coupling, will be described here in the next section.

3. Testing NTV physics with the particle simulations

In this section, numerical tests of essential NTV features such as the $1/\nu$ and $\nu \sqrt{\nu}$ behaviours, the superbanana-plateau (SBP), the bounce-harmonic resonances, and the toroidal mode decoupling are presented using the particle simulations in the zero and finite $\vec{E} \times \vec{B}$.

3.1. Field resonance

A magnetic braking is often assumed to be driven mainly by non-resonant magnetic perturbations. This supposition, however, can be misleading, since particle orbits can be repetitively distorted at most when the field patterns are resonant with orbit patterns, that is, $m - nq \sim 0$. This can be also seen in various semi-analytic methods, as the bounce-averaged integral for (m, n) perturbation becomes the largest in such a condition. This field resonance has been tested in POCA, by estimating NTV for each single harmonics (m, n) of the actual variation in the field strength in each flux surface having a safety factor q . Here the magnetic perturbations $\delta B/B_0 = \delta_{mn}(\psi_n) \cos(m\theta - n\varphi)$ with $\delta_{mn}(\psi_n) = 0.02\psi_n^2$ are applied to a background plasma of $\nu_* \sim 1.0$ in [16], which

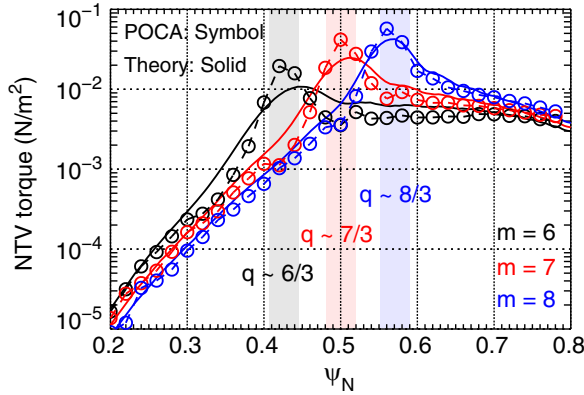


Figure 2. NTV torque profiles by ($m = 6, 7, 8, n = 3$) modes. Strong NTV peaks appear at the resonant flux surfaces where $q = 6/3, 7/3,$ and $8/3$ for each poloidal mode number.

is in the $1/\nu$ regime. Fixing the toroidal mode number as $n = 3$, the poloidal mode number is varied by $m = 6, 7,$ and 8 to change the resonant mode. The $\vec{E} \times \vec{B}$ rotation is set to be zero for simplicity here.

As shown in figure 2, strong NTV peaks appear nearby the resonant flux surfaces at $q = 6/3, 7/3,$ and $8/3$ corresponding to the applied poloidal mode numbers. The peak flux surface is shifted by the applied mode, and the NTV is dominated by the resonant perturbation, while NTVs rapidly drop at the off-resonant flux surfaces. Note much stronger torques are found at the edge rather than the core, but this is just due to the envelope change by the field attenuation from the edge to the core. One can also see that overall trend of NTV profiles by POCA is highly consistent with the combined NTV calculations in this high aspect-ratio and the low β case, as described in [16].

A subtlety about the field resonance, however, still exists due to plasma response to externally applied magnetic perturbations. Resonant components of external magnetic perturbations typically produce stronger plasma response than non-resonant components. They either can be too much disruptive to see NTV effects or can be strongly attenuated by screening effects, depending on radial locations of flux surfaces and stability characteristics of plasma targets. This interference is not expected for non-resonant external perturbations and thus NTV effects can be seen more apparently. However, if external perturbations are too much non-resonant, i.e., very far from the resonant condition $m - nq \sim 0$, their effects can be too weak or noisy to produce NTV. Note there are extra complications in bounce-harmonic resonances, i.e., $m - nq \pm \ell \sim 0$. It will be interesting in the future to examine a proper decomposition of external magnetic perturbations by their relative importance on NTV, but this subtle balance should be considered with a self-consistent plasma response model.

3.2. Collisionality dependency of NTV with finite $\vec{E} \times \vec{B}$

NTV physics strongly depends on collisionality and toroidal precession rates, as NTV regimes are frequently defined by these two parameters. Mainly two distinct trends have been predicted; $1/\nu$ [11] dependency in relatively high collisionality and $\nu_- \sqrt{\nu}$ [13] roll-over when collisionality becomes lower

than precession. When precession is very low, $1/\nu$ regime can be extended to lower collisionality regime and connected to so-called SBP regime, where precession can be zeroed by cancellation between electric $\vec{E} \times \vec{B}$ and magnetic precession. On the other hand, when precession becomes strong enough, bounce-harmonic resonances can occur and largely enhance transport.

In order to test these parametric dependencies, POCA simulations were performed to scan NTV in a wide range of collisionality $10^{-4} < \nu_* < 10^4$ in three different $\vec{E} \times \vec{B}$ precession rates as shown in figure 3. Results were also compared with combined NTV calculations, which can provide theoretically predicted trends reasonably well in simplified geometry as tested here. The collisionality, ν_* has been scanned by multiplying density by a constant while dividing temperature by the same constant for the plasmas in figure 2(a) and [16] with $n_0 = 2.0 \times 10^{17} \text{ m}^{-3}$, $T_0 = 0.5 \text{ keV}$. Thus, the total pressure was not affected by the collisionality variation in the scan. The applied field is $(m, n) = (7, 3)$ and NTV torque density is estimated at $\psi_n = 0.45$ which is close to the resonant flux surface.

POCA and combined NTV results both show the fundamental $1/\nu$ behaviours in high collisionality and predicted transition to $\nu_- \sqrt{\nu}$ regime when $\vec{E} \times \vec{B}$ is finite. There are nonetheless quantitative differences between two results, which becomes more apparent in higher collisionality where one can see POCA predicts larger NTV than combined NTV in general. This is because combined NTV only includes trapped particle effects, but in higher collisionality, the fraction of trapped particles becomes smaller and passing particle effects can be dominant in transport process.

The zero $\vec{E} \times \vec{B}$ limit, figure 3(a), has even an important qualitative discrepancy between two results. When collisionality is sufficiently low, POCA shows SBP behaviour that has been predicted from theory [22]. On the other hand, combined NTV does not show SBP as already claimed once by numerical testing work with a global particle simulation code, FORTEC-3D [20]. The failure in combined NTV for SBP is due to geometric and pitch-angle simplifications in magnetic precession, but the difference between POCA and FORTEC-3D results possibly implies that SBP may be a local effect and may be not as strong as expected due to its sharp resonant conditions. This issue has been discussed in the recent paper by Logan *et al* [23], which reported a recovery of SBP regime by eliminating the large aspect-ratio approximation in the combined NTV theory. As argued in [23], open issues remain in the SBP regime of NTV and it is another important subject that can be tested by a dedicated study combining the local and global particle simulation, even though it is beyond the scope of this paper. It is also notable that the lowest collisionality in the collisionality scan almost touches a limit of local approach where narrow annulus is defined for a home flux surface, thus it would be very difficult to further reduce the collisionality to test superbanana regime due to large banana orbit width of particles with very high thermal velocity. This is one of the limitations of local particle simulation, implying a necessity of a global approach. This issue will be further studied in the future, as NTV prediction in low collisionality is critical for the next-step devices and ITER.

With a high $\vec{E} \times \vec{B}$, figure 3(c), both calculations show strong enhancement of NTV by bounce-harmonic resonances

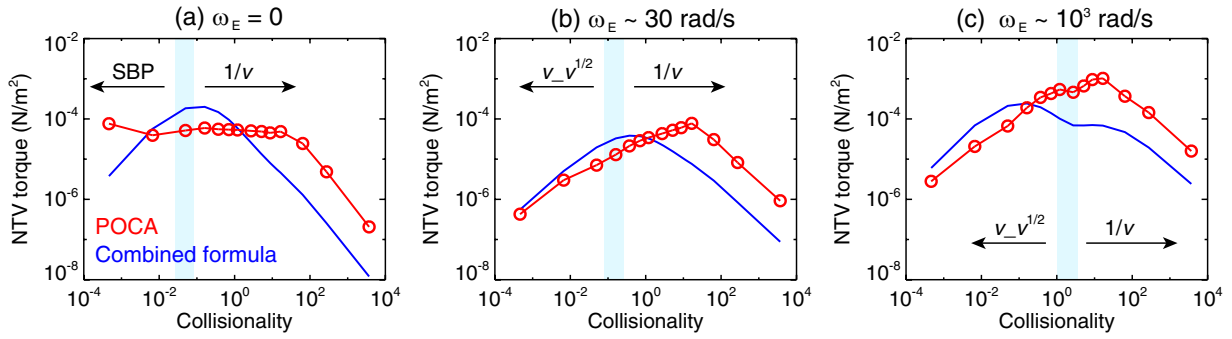


Figure 3. Comparison of NTV between POCA (red-symbol) and combined formula (blue-solid) as a function of collisionality with fixed $\vec{E} \times \vec{B}$ frequency at (a) $\omega_E = 0$, (b) $\omega_E \sim 30 \text{ rad s}^{-1}$, and (c) $\omega_E \sim 10^3 \text{ rad s}^{-1}$. Shaded is the theoretically estimated boundary (a) for SBP and $1/\nu$ regime, and (b), (c) for $\nu_{-\sqrt{\nu}}$ and $1/\nu$ regime.

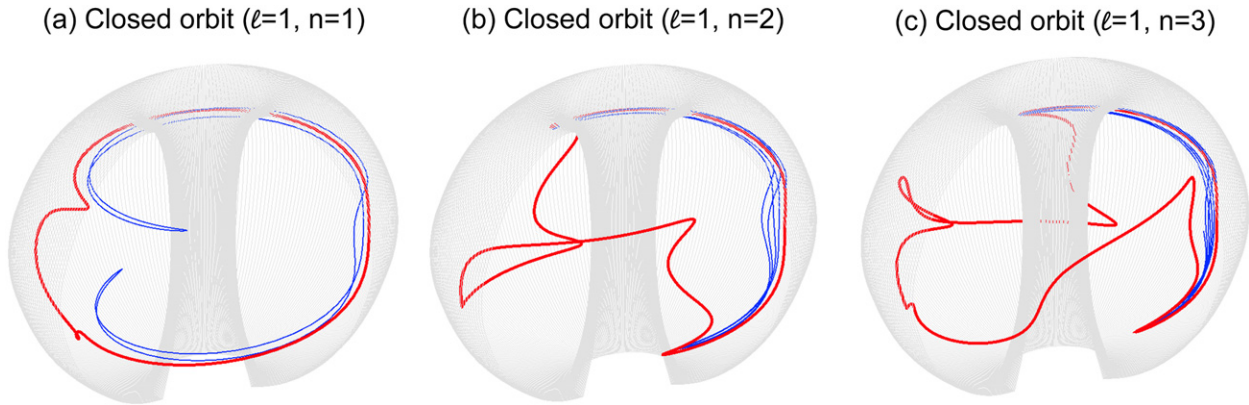


Figure 4. 3D particle trajectories of the closed orbit with $\vec{E} \times \vec{B}$ (red) compared to the original banana orbit (blue) in NSTX. The closed orbit of the ℓ -class particle toroidally circulates ℓ cycles for n bounces as shown for (a) $(\ell, n) = (1, 1)$, (b) $(1, 2)$, and (c) $(1, 3)$.

[14, 25, 26]. Since the bounce frequency is much higher than $\vec{E} \times \vec{B}$ frequency in the whole range of collisionality in figure 3(b), the bounce-harmonic resonances hardly occur. On the other hand, the bounce frequency is largely similar to $\vec{E} \times \vec{B}$ frequency in figure 3(c), thus the bounce-harmonic resonances take effects as indicated by overall increment of NTV torque. The resonant peaks can also be seen in (c) by the bumps and variations in addition to the expected ν to $\nu_{-\sqrt{\nu}}$ trends, although the peak values and positions are not perfectly consistent. The importance of bounce-harmonic resonances have been recently verified by simulations [21] and observed in experiments [27]. As discussed in references, the perpendicular motion by $\vec{E} \times \vec{B}$ precession can largely suppress radial particle drifts by phase-mixing, but the phase-mixing can disappear in bounce-harmonic resonances as the $\vec{E} \times \vec{B}$ precession is large enough to resonate with the parallel motion [21]. Together with the SBP resonance with small $\vec{E} \times \vec{B}$ [15, 22], the bounce-harmonic resonance is an important mechanism enhancing NTV transport. It should be noted that collisionality boundaries between SBP, $1/\nu$, and $\nu_{-\sqrt{\nu}}$ regimes in the POCA simulation are found to be shifted from the theoretical estimations [24], which can be caused by overlapping of collisionality regimes due to different pitch-angle and energy of particles in the Maxwellian distribution.

In [21], closed orbits were newly found in the simplified large aspect-ratio tokamak configurations with circular-shaped plasmas. The closed orbits of ℓ -class particles toroidally

circulates ℓ cycles for n bounces when the rotational resonance condition, $\ell\omega_b \sim n\omega_E$ is satisfied. Here, ℓ is the digit representing the bouncing class of particles, ω_b is the bounce frequency, and ω_E is the $\vec{E} \times \vec{B}$ electric precession frequency. We found such closed orbits in the real tokamak configuration of NSTX as presented in figure 4. A single-harmonic perturbation was applied to simplify the magnetic perturbation as in the previous section, and the closed orbits were formed on the corresponding flux surfaces satisfying the resonant field condition $m - nq \pm \ell = 0$, as described in [21].

One can notice that the closed orbits can indeed exist in the real tokamak configuration and their trajectories are even more complex. The $\vec{E} \times \vec{B}$ precessions almost always exist in practice and make the particle orbits much more complicated compared to the zero- $\vec{E} \times \vec{B}$ or the single-harmonic case. The bounce-harmonic resonances always occur for a fraction of particles in the finite $\vec{E} \times \vec{B}$ due to Maxwellian energy distribution, and on every surface due to multi-harmonic magnetic perturbations. This bounce-harmonic effect is automatically included in the POCA simulation by the guiding-centre drift motions so that the orbit closing and evolution by $\vec{E} \times \vec{B}$ are realistically taken into account. The bounce-harmonic resonances can be easily dominant in the magnetic braking experiments with the finite $\vec{E} \times \vec{B}$, and thus it is important to include them in the NTV calculations. These will be further discussed for the practical magnetic braking discharges in section 5.

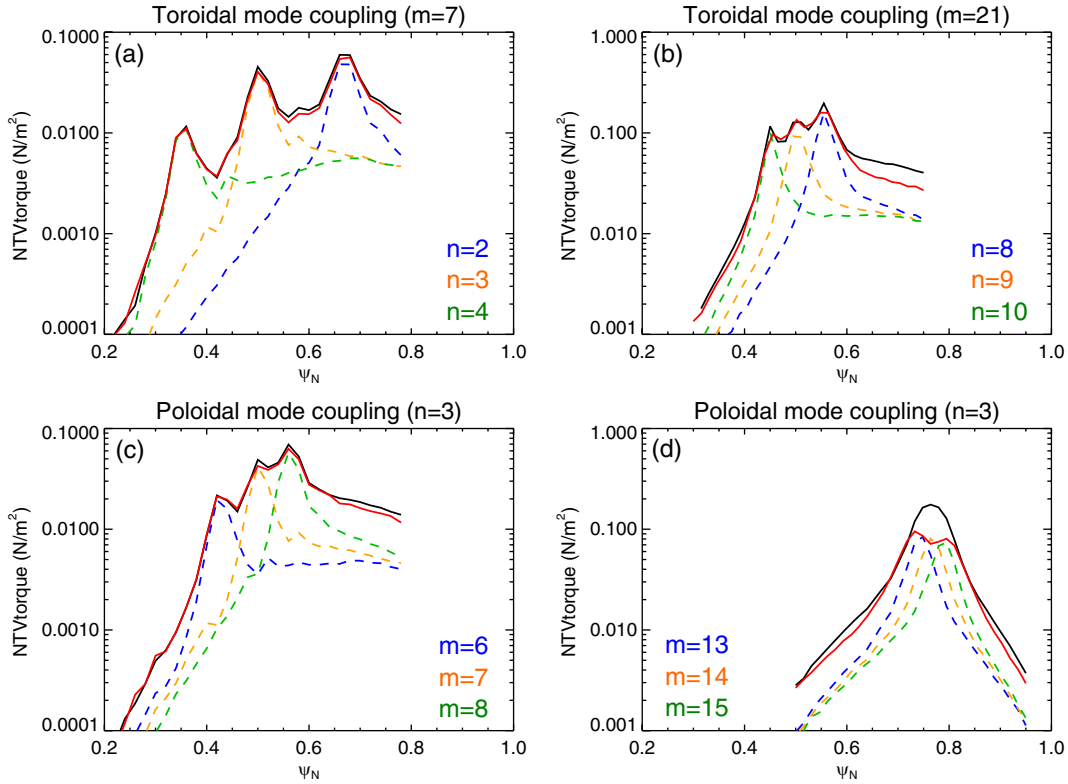


Figure 5. Comparisons of NTV profiles between three-mode (red) and linear sum of single-mode (black) perturbations. Three-modes are considered with the fixed poloidal mode for (a) and (b), and the fixed toroidal mode for (c) and (d). Broken curves indicate the NTV profiles by single-mode perturbation, and black solid curve does their sum.

3.3. Toroidal and poloidal mode coupling

NTV theory in tokamaks predict poloidal mode coupling but toroidal mode decoupling, due to the quasi-linear nature of treatment on unperturbed axisymmetric magnetic field [28, 29]. This mode coupling issue is critical in some practical cases, such as tritium-breeding test blanket modules (TBMs) in ITER, which are expected to produce multi-toroidal and poloidal harmonic perturbations [30]. For test, we applied three-mode magnetic perturbations expressed as $\delta B/B_0 = \sum \delta_{mn}(\psi_n) \cos(m\theta - n\varphi)$ to the model plasma in section 3.1. The resulting NTV torque was compared with the linear NTV sum of three single-mode perturbations with the same harmonics.

Simulation results are presented in figure 5, showing indeed little to no toroidal mode coupling effect. Figures 5(a) and (b) are the comparison of NTV profiles, where three-mode in toroidal harmonics was considered with a fixed poloidal mode. The mode numbers were selected to control the distance between the resonant flux surfaces to the applied perturbations, thus figure 5(a) is the case for a large distance between the peak NTVs while figure 5(b) is the one for a small gap. It is found that the NTV profiles from the three-mode harmonics is almost the same as the sum of single modes regardless of the gap between the resonant surfaces.

Poloidal mode coupling effect was also checked in a similar manner but by changing the poloidal mode number with a fixed toroidal mode number. By comparing figures 5(c) and (d), one can find the poloidal modes are decoupled when the gap distance is large in 5(c) but can be coupled when the

gap is reduced in figure 5(d). Figure 5(d) shows that the NTV density from the three-mode harmonics is largely different from the linear sum of the single-mode especially around the resonant flux surfaces, indicating nonlinear response of NTV to the multi-poloidal harmonics and thereby strong poloidal mode coupling [31].

4. Reconstruction of perturbed magnetic field δB for particle simulation

An accurate calculation of the perturbed magnetic field δB is the key to the precise NTV estimation. The spatial structure of δB must be consistent with nested flux surface everywhere, which is also one of the fundamental assumptions of NTV theories. POCA code uses δB computed by IPEC, which is a well-known ideal perturbed equilibrium code, capable of computing δB with an ideal plasma response [32]. When ideal plasma response is included for this, however, δB profiles can be very complicated especially around the rational surfaces due to the ideal constraints for the nested flux surfaces. These fine structures of δB are unnecessary for guiding-centre orbits, especially for ions. Thus, POCA uses Chebyshev polynomials radially, and Fourier modes poloidally and toroidally to represent 3D structure of the magnetic field obtained with IPEC. Then, δB is expressed as

$$\delta B(\psi_n) = \sum_{m,n} \sum_j^{n_c} a_j \cos[j \cos^{-1}(x)] \cos(m\theta - n\varphi) + b_j \cos[j \cos^{-1}(x)] \sin(m\theta - n\varphi), \quad (5)$$

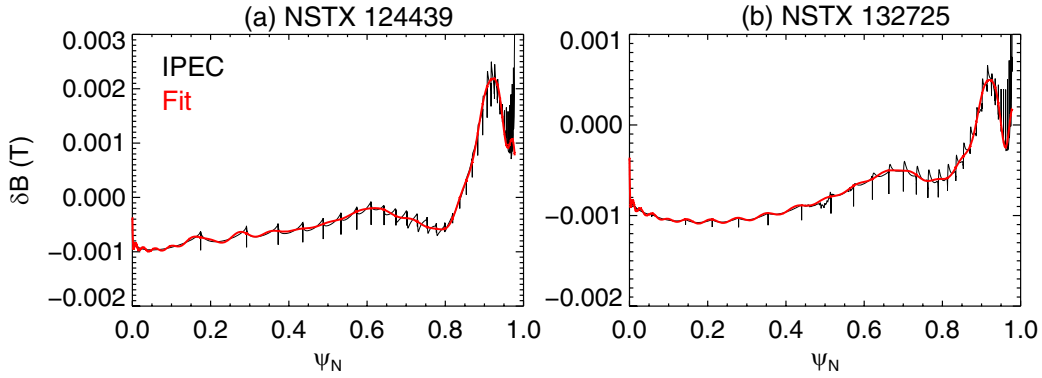


Figure 6. Comparison of non-axisymmetric magnetic field profiles between IPEC and fitting with Chebyshev polynomials for NSTX discharge (a) 124 439 and (b) 132 725. Profiles are taken at $(\theta, \varphi) = (0, 0)$ with $n_c = 20$. Fittings efficiently smooth the nonphysical peaks but reflect overall features of the original IPEC calculation well.

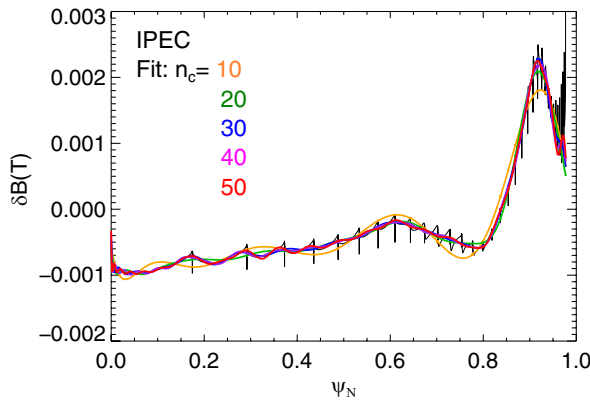


Figure 7. Sensitivity of Chebyshev fitting to the degree of polynomials. δB profiles for NSTX 124 439 in figure 6(a) are taken.

where n_c is the degree of polynomials, a_j and b_j are the Chebyshev coefficients for each degree j , and $x = 2\psi_n - 1$.

Figure 6 shows comparisons of the δB profiles between original IPEC result and fitting in the NSTX discharges, where the radial profiles are taken at $(\theta, \varphi) = (0, 0)$ with $n_c = 20$. One can notice that the fitted profiles reflect overall trend of complex field structure very well, even though the strong peaks at the rational flux surfaces are effectively smoothed. The fitting function is sensitive to the degree of Chebyshev polynomials n_c as seen in figure 7, where each fitting curve is drawn for different n_c . A lower degree fitting roughly follows the original δB with wobbling, and shows a poor fitting quality at the edge containing dense rational surfaces. On the other hand, high degree gives a better fitting to the IPEC calculation, so that it follows very well the rapid δB changes at the rational surfaces and effectively smoothes unnecessary resonant peaks. The degree of polynomials of $n_c \geq 20$ is found to provide good resolutions for the examples, but this can depend on the discharge condition. Note higher degree usually guarantees an accurate fitting but requires longer simulation time. In the following experimental analyses, $n_c = 20$ is used to simultaneously satisfy the computational accuracy and efficiency.

5. NTV calculations in magnetic braking experiments

In parallel with numerical verifications as described, POCA has been actively applied to magnetic braking discharges in DIII-D and NSTX. For the simulations, IPEC first computes the perturbed magnetic field δB with the ideal plasma response, and then POCA calculates the NTV using the δB from equation (5) and kinetic profile measurements for temperature, density and rotation. The electric potential profile in equation (3) is obtained from a radial force balance equation $\nabla p = eN(\vec{E} + \vec{u} \times \vec{B})$, which is given by measurements. It was from measured pressure and toroidal rotation, and neoclassical estimation of poloidal rotation in NSTX, while the poloidal rotation was also measured in DIII-D. Note the POCA uses a given potential profile but does not evolve it self-consistently, thus errors in the electric potential always remain impacting on the NTV torque. This could be improved by self-consistent calculation of the electric potential in the future.

Our test cases are essentially identical to ones previously computed by combined NTV calculations [14] and published in [33] for DIII-D and in [34] for NSTX, but with further updates in several aspects. (1) Previous calculations used regular spatial grid with 100–200 points. This is not even close to the original IPEC spatial resolution of grids, which are adaptive and easily have $\sim 10^4$ grid points. New calculations have the full IPEC grid as one can see clear resonant peaks in every rational surface. (2) The integration in the velocity space is also increased in order to capture sharp peaks of bounce-harmonic resonances in the energy space. (3) Last, especially for NSTX, IPEC equilibrium calculation itself has been improved more reliably for high $n > 2$, by changing magnetic coordinates from Hamada to Boozer or hybrid and thus allow Jacobian to follow the large changes of $1/B^2$ in NSTX, up to two orders of magnitudes in a flux surface. Nevertheless, conclusions in the previous work remain the same, as [34] showed that the combined NTV based on Lagrangian δB in IPEC improved the consistency between theory and experiment within an order of magnitude but the accuracy is still not sufficient to predict the damping rates in details. Here POCA suggests another possible improvement in the NTV prediction.

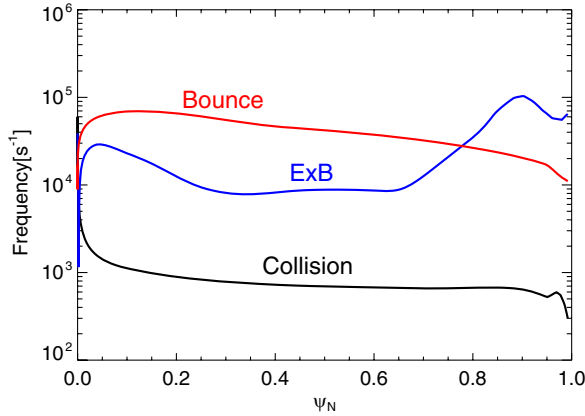


Figure 8. Frequency profiles of ion collision, electric precession, and ion bounce motion for the DIII-D 145117. It is indicated that the plasma is in the $\nu_{-}\sqrt{\nu}$ regime, however, bounce-harmonic resonance can be important at the edge.

5.1. QH-mode discharge in DIII-D

A QH-mode discharge 145117 in DIII-D tokamak was selected to validate the NTV calculation using POCA. The QH-mode is believed to be accessible by strong rotational shears at the edge, and non-axisymmetric magnetic perturbations have been utilized to produce favourable rotation profiles [35]. For this discharge, non-resonant $n = 3$ non-axisymmetric magnetic perturbations were applied using I-coil and C-coil to the neutral beam injection (NBI)-heated plasma ($I_p = 1.1$ MA, $B_T = 1.95$ T), so the net-NBI torque at the ITER-relevant level was achieved with the magnetic braking by the NTV torque [33].

Collisionality regime of this discharge can be estimated by comparing the collision frequency, ν/ϵ with the electric precession frequency, $nq\omega_E$ [36]. Figure 8 presents the profiles of these frequencies for the discharge together with the bounce frequency of trapped ions, $\omega_b = \omega_t\pi\sqrt{\epsilon}/4\sqrt{2}$, where ω_t is the transit frequency. It is indicated that the plasma is in the $\nu_{-}\sqrt{\nu}$ regime since $\nu/\epsilon \ll nq\omega_E$. However, one can expect the bounce-harmonic resonances can take effects at the edge where $\ell\omega_b \sim n\omega_E$ can be satisfied [14, 21], thus they can drive stronger NTV than predicted by the $\nu_{-}\sqrt{\nu}$ theory.

Total NTV torque in the discharge was measured using an angular momentum balance equation and estimated at ~ 3 N m, as described in [33]. There is no measurement for the NTV profile in this discharge, therefore the total NTV is used for a comparison with the simulation. Figure 9 presents the calculation results of NTV torque profile by POCA and combined NTV, and shows a good agreement in the profile and amplitude. The POCA calculation predicts stronger NTV at the core and weaker NTV at the edge than the theory, but the overall trend is consistent to each other. Both calculations agree well with the experimental estimation for the total NTV torque, i.e. 2.94 N m by POCA and 2.64 N m by theory, indicating the successful application of the developed particle simulation. Strong peaks in the theory calculation in figure 9 are due to the amplification of NTV at the rational surfaces by $\tau_\phi \propto (\delta B)^2$ since the theory uses δB directly from IPEC. It is not yet entirely clear why a NTV peak around $\psi_N = 0.2$ appears in the POCA simulation. It would be possible that finite orbit width in the POCA simulation causes a shift of

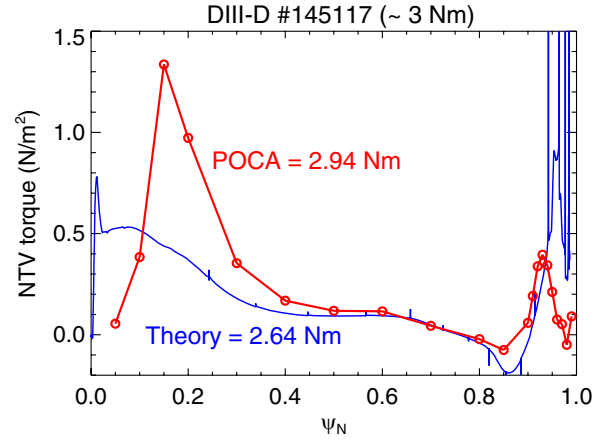


Figure 9. NTV profiles for DIII-D discharge 145117 by POCA (red) and the combined theory (blue). Both calculations provide a reasonable prediction in total NTV torque (2.94 N m by POCA, 2.64 N m by theory), which is estimated at ~ 3 N m in the experiment.

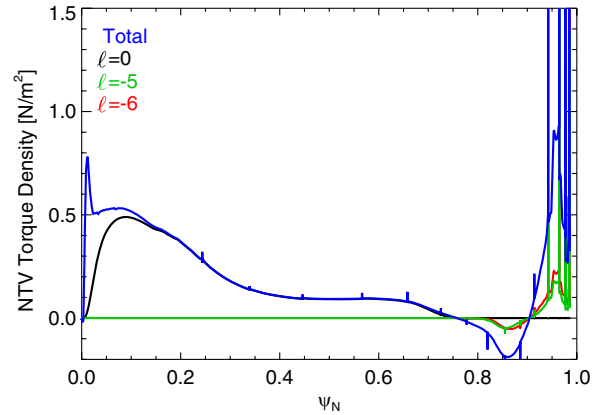


Figure 10. NTV profiles calculated by the combined formula for dominant ℓ -classes. Bounce-harmonic resonances are found to be important only in the pedestal due to slow toroidal rotation in the discharge.

NTV peak near the axis in the combined NTV result or passing particles only included in the POCA might play a role on the peak as discussed in [37]. It is currently not possible to find a clear answer in this paper, but would be available in the future through developing numerical and theoretical methods to quantify the effects of finite orbit width and passing particles.

It is interesting to notice that the combined theory calculation indicates $\ell = 0$ class particles are dominant in driving the NTV torque for the analysed discharge as shown in figure 10, where the contributions from each ℓ -class particles for the NTV are separately displayed. The bounce-harmonic resonances are found to be very small at the core but become strong at the edge by $\ell = -5$ and -6 class particles, which is consistent with the regime analysis in figure 8.

5.2. NSTX discharges with fast toroidal rotation

Two magnetic braking discharges 124439 and 132729 for NSTX were analysed using POCA. Axisymmetric equilibria are reconstructed using LRDFIT [38]. The toroidal rotation speed, u_ϕ is measured by charge exchange

recombination spectroscopy (CHERS) based on carbon impurities, assuming the CHERS represents the main ion rotation. The poloidal rotation is neglected in the simulations due to the fast toroidal rotation in the selected discharges.

For the NSTX discharges, NTV torque profiles were measured from toroidal rotation changes by the magnetic braking, as described in [34]. In the discharge 124 439, where $\kappa = 2.3$, $I_p = 0.8$ MA, and $B_T = 0.45$ T in the lower single null configuration, the toroidal rotation was observed to damp and relax to a different rotational equilibrium after $n = 3$ magnetic braking was fully applied by EF/RWM coils. Particle transport was not changed even though the non-axisymmetric fields produce a strong momentum transport, and it was clearly indicated that the damping is purely driven by the $n = 3$ magnetic braking.

A reference discharge, where the plasma is identical except the magnetic braking, is useful to estimate the toroidal rotational damping rate, ν_{damp} . The rotational damping rate can be measured by calculating the rotation changes of the target discharge compared to the reference shot. A short time period after turning on EF/RWM coils is considered so that an exponential decay of the rotation can be linearized [34]. Then, the NTV is calculated from the damping rate using

$$\tau_\varphi \approx \nu_{\text{damp}} u_N^\varphi R M N, \quad (6)$$

where M is the mass of a species, N is the density, R is the major radius, and u_N^φ is the neoclassical toroidal flow. The neoclassical toroidal flow is defined by

$$u_N^\varphi \equiv u_\varphi + C_N \left| \frac{1}{eZ} \frac{dT}{d\chi} \right|, \quad (7)$$

where χ is the poloidal flux function. The second term of equation (7) represents a neoclassical offset flow with $C_N \approx 3.5$ for $1/\nu$ regime, $C_N \approx 0.92$ for $\nu_{-}\sqrt{\nu}$ regime, and $C_N \approx 2.0$ for combined regime [11, 14]. The offset flow has not been measured in NSTX, so it is analytically calculated using equation (7).

The plasma regimes for the discharge can be estimated from figure 11, where the collision, the electric precession, and the bounce frequencies are compared. One can find the plasma is in the $\nu_{-}\sqrt{\nu}$ regime at the core and in the $1/\nu$ regime at the edge. However, the regimes are not identified as clearly as in the DIII-D case. The bounce frequency is in the comparable range to the electric precession frequency in the entire region, thus one can easily expect strong bounce-harmonic resonances. Such impacts of the bounce-harmonic resonances are clearly found from the NTV torque profiles for each ℓ -class particles calculated by the combined NTV. Figure 12 shows that the $\ell = 0$ class particles in the $1/\nu$ regime have local contributions at the edge ($\psi_N > 0.8$), as indicated by highest collision frequency, $\nu/\epsilon > nq\omega_E$, ω_E in figure 11. However, the bounce-harmonic resonances by $\ell = 3, 4$, and 5 class particles drive much stronger NTV than the $\ell = 0$ class particles at the core ($\psi_N < 0.8$), where the plasmas are largely in the $\nu_{-}\sqrt{\nu}$.

Such strong bounce-harmonic resonances cause significant discrepancies among POCA and combined NTV calculations, and even measurements. Figure 13(a) shows a comparison of the rotational damping rate between the measurement

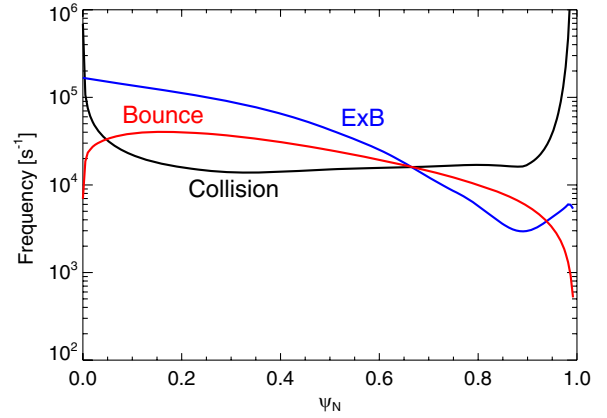


Figure 11. Frequency profiles of the ion collision, the electric precession, and the ion bounce motion for the NSTX 124439. It is indicated that the plasma is in $\nu_{-}\sqrt{\nu}$ regime at the core and in $1/\nu$ regime at the edge. Bounce-harmonic resonances take dominant effects in the whole region due to fast toroidal rotation.

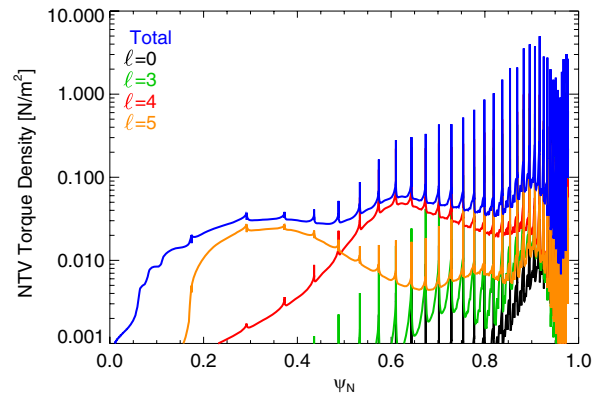


Figure 12. NTV profiles calculated by the combined formula for dominant ℓ -classes. Bounce-harmonic resonances are found to take dominant effects in the overall region due to fast toroidal rotation, and $\ell = 0$ particles take local effects at the edge.

and POCA, drawn together with a prediction by combined formula. Interestingly, the NTV torque profile by POCA is similar to the theory calculation in shape but much stronger in amplitude by an order of magnitude. On the other hand, the POCA calculation roughly shows agreement with the estimated damping profile at the outer region at $\psi_N > 0.5$. Large discrepancies are still found at $\psi_N < 0.5$. Figure 13(b) shows the NTV profiles by POCA and the measurement. Similarly, POCA indicates weaker NTV at inner region and stronger at outer region. Note that the POCA simulations have predicted stronger bounce-harmonic resonances and thereby stronger NTV than the theory in the fast rotating plasmas [21]. Underestimated NTV by the combined theory would be consistent to the expectation that the analytic theory becomes less precise in fast rotating plasmas due to strong distortions in particle orbits by fast precession. POCA gives 2.7 N m in total NTV torque, which is more comparable to the experimental value 3.5 N m than the combined theory prediction of 0.55 N m.

Another NSTX discharge 132729, where $I_p = 1.1$ MA and $B_T = 0.55$ T, was analysed for the NTV in the same manner. For this discharge, 750 A of current was run in the NSTX to produce strong $n = 3$ magnetic braking, as

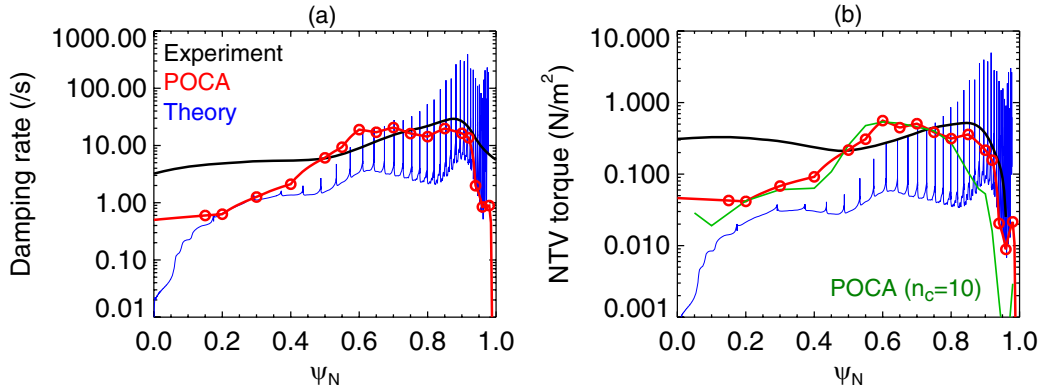


Figure 13. Comparison of (a) rotational damping rate and (b) NTV torque profile between measurement (black), POCA (red) and theory (blue) for NSTX discharge 124 439. Total NTV torque is measured at 3.5 N m, and agrees well with 2.7 N m from POCA in spite of discrepancies in the profile. NTV profile by POCA with $n_c = 10$ is drawn for comparison (green), showing a poor agreement at the edge due to less accurate fitting of δB .

described in [39]. In this discharge, the plasma is in the similar collisionality regime with 124 439, and strong bounce-harmonic resonances are expected as well due to the fast toroidal rotation. Figure 14 presents comparisons of the damping rate and NTV torque profiles for 132 729. Large discrepancies are found in both profiles, where POCA predicts weaker NTV at the inner and edge region and stronger NTV elsewhere. The disagreements in the profiles are more significant at the core, which might be caused by experimental and numerical uncertainties as will be discussed in the next section. However, it is interesting to find that the total NTV torque with POCA is still comparable to the measurement due to sub-dominant contribution of the core region to the total torque; POCA gives 3.5 N m and the experiment 5.1 N m. Theory still largely underestimate the total torque at 0.44 N m. One can notice that only measurement shows strong NTV at the edge unlike theory and simulation, even though NTV drops at the edge are consistent in figures 9 and 13 for other discharges. This could be due to the sensitivity in measuring the rotational damping rate. The toroidal rotation measurement in the discharge 132729 was relatively unclear compared to 124439, which might cause an abnormally large NTV at the core as well as at the boundary. Detailed transport analysis cross-checking other diagnostics will be required to resolve these uncertainties.

It is notable that the NSTX experiment has many difficulties in calculating the NTV torque compared to the DIII-D configuration, which may result in the large discrepancies between theory, simulation, and measurements. Theoretical approximations such as the large aspect-ratio expansion and the zero-orbit-width assumption become crucial and invalid for NSTX due to the low aspect-ratio and weak toroidal magnetic field. In addition, the bounce-harmonic resonance effects become stronger than theory prediction when the rotation is fast in NSTX since particle transport by bounce-harmonic resonances can be largely underestimated without finite orbit width [21]. Passing particle effects excluded in theory have also non-negligible contributions on stronger NTV predicted by POCA simulations even in the large aspect-ratio [37]. These elements all make the comparison of the simulation with the measurements more complicated, but should be thoroughly tested to validate particle simulations and NTV in experiments.

6. Issues for improving NTV prediction

The NTV torque can be measured from the toroidal angular momentum balance and/or the toroidal rotation diagnostics, but there are still many uncertainties that must be improved in the future. First, separate transport calculations such as TRANSP analysis in [33] rather than the rotational damping rate are required in order to obtain the total NTV from the toroidal angular momentum equation. However, one should be careful when performing such transport analyses because they contain their own uncertainties. For instance, the intrinsic torque caused by turbulence or internal magnetohydrodynamic (MHD) modes should be properly treated in the momentum balance equation. Second, the damping rate measured by carbon ion rotation using CHERS can be different from that of main ion due to a different responding time to the non-axisymmetric perturbations. Also, an intrinsic assumption such as $u_\phi \approx u_{\text{carbon}}$ needs to be confirmed. Third, neoclassical offset flow should be measured. When estimating NTV torque profile from the measured damping rate, theoretically calculated neoclassical offset flow was used due to the absence of measurements. Generally, the offset flow can be strong at the H-mode edge due to a steep temperature gradient, so it can greatly enhance the NTV value at the edge. If one ignores the offset flow in the neoclassical toroidal flow in equation (7), equation (6) gives reduced torques in the edge and smaller total values of 1.5 N m for 124439 and 2.36 N m for 132729, implying the importance of offset rotation in the NTV measurement. Thus, more robust diagnostics for the toroidal rotation and offset flow are necessary to eliminate such uncertainties. The neoclassical offset may be measured or calculated with a series of experiments or simulations scanning the NTV torque with toroidal plasma rotation, which could be helpful to validate the coefficient C_N in the neoclassical theory.

For the simulation, it should be noted that the ideal perturbed equilibria can fail in the high β plasmas and strong NTV braking, as in the NSTX discharges. The validity of the ideal perturbed equilibria has been theoretically discussed using dimensionless parameters in [4]; $s \equiv -\delta W/\delta W_v$ and $\alpha \equiv -T_\phi/2N\delta W_v$ with δW the total energy, δW_v the required energy to produce the same perturbation without plasma, and T_ϕ the total NTV torque. This theory indicates that

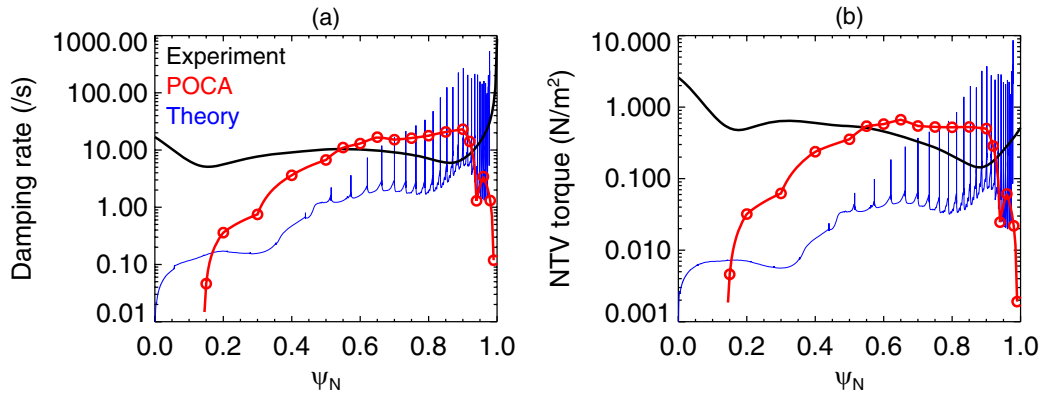


Figure 14. Comparison of (a) the rotational damping rate and (b) the NTV torque profile among measurement (black), POCA (red), and theory (blue) for NSTX discharge 132729.

the ideal perturbed equilibria can be valid when $|s| > |\alpha|$, corresponding to weak NTV. Otherwise, a shielding effect associated with the toroidal torque becomes crucial to prevent a penetration of the perturbed magnetic fields. In this sense, the δB from the ideal perturbed equilibria gives an inconsistent NTV by the ignorance of such shielding effects.

The studied NSTX discharges satisfy $|s| > |\alpha|$, indicating the presented NTV based on ideal δB is globally valid and explaining the rough quantitative agreements in the total torque. However, the NTV effects on perturbed equilibria in fact can occur differently depending on locations. The strong NTV spikes around the rational surfaces can induce currents associated with NTV and can change the field penetration and consequently δB in the perturbed equilibrium. These local NTV effects should be considered particularly at the edge, which is generally dense with the rational surfaces as shown in figures 13 and 14. The self-consistent calculation of δB including the non-ideal plasma response will eventually be required to obtain self-consistent predictions of the perturbed equilibria and thereby the NTV transport. It can be achieved from a general perturbed equilibrium code solving 3D force balance with the perturbed anisotropic tensor pressure.

7. Conclusions

A Particle Orbit Code for Anisotropic pressures, POCA has been developed for the accurate calculation of δf by guiding-centre drift given non-axisymmetric equilibria. NTV analysis has been carried out using analytic and practical non-axisymmetric magnetic field perturbations. Simulations with the analytic perturbation consistently show the NTV physics such as the strong field and rotational resonances, and toroidal mode decoupling in the NTV transport. POCA applications to magnetic braking experiments in DIII-D and NSTX show better quantitative predictions than analytic calculations in total NTV torque, however large discrepancies remain in the detailed NTV profiles, especially for NSTX discharges. More robust estimation of NTV is necessary in the future, and it can be achieved by dedicated rotation measurement and integrated momentum transport analysis with reliable torque sources. Validation studies of the particle simulations should continue on the various plasma regimes in the various tokamak machines as well.

Theoretical and numerical uncertainties intrinsically contained in the non-axisymmetric magnetic perturbations could be eventually overcome through general perturbed equilibria. The calculation based on ideal perturbed equilibria breaks down in the high β plasmas and in strong magnetic braking cases. Penetration of the perturbed field into the plasma can be significantly changed by the non-ideal plasma response associated with the strong local NTV. Thus, the self-consistent δB by a general perturbed equilibria is required to achieve more precise NTV prediction. The self-consistent NTV calculation can be accomplished throughout an integrated calculation of the transport and the General Perturbed Equilibrium Code (GPEC), which is actively under way.

The data contained in the figures in this paper can be found at http://nstx.pppl.gov/DragNDrop/Publications_Presentations/Publications/2014%20Data.

Acknowledgments

This work was supported by DOE Contract No DE-AC02-09CH11466 (PPPL) and No DE-FC02-04ER54698 (GA).

References

- [1] Galeev A.A., Sagdeev R.Z., Furth H.P. and Rosenbluth M.N. 1969 *Phys. Rev. Lett.* **22** 511
- [2] Goldston R.J., White R.B. and Boozer A.H. 1981 *Phys. Rev. Lett.* **47** 647
- [3] Boozer A.H. 1980 *Phys. Fluids* **23** 2283
- [4] Boozer A.H. 2001 *Phys. Rev. Lett.* **86** 5059
- [5] Sabbagh S.A. et al 2006 *Nucl. Fusion* **46** 635
- [6] Garofalo A.M., Burrell K.H., DeBoo J.C., deGrassie J.S., Jackson G.L., Lanctot M., Reimerdes H., Schaffer M.J., Solomon W.M. and Strait E.J. 2008 *Phys. Rev. Lett.* **101** 195005
- [7] Evans T.E. et al 2004 *Phys. Rev. Lett.* **92** 235003
- [8] Sabbagh S.A., Bell R.E., Menard J.E., Gates D.A., Sontag A.C., Bialek J.M., LeBlanc B.P., Levinton F.M., Tritz K. and Yuh H. 2006 *Phys. Rev. Lett.* **97** 045004
- [9] Callen J.D. 2011 *Nucl. Fusion* **51** 094026
- [10] Shaing K.C. and Callen J.D. 1983 *Phys. Fluids* **26** 3315
- [11] Shaing K.C. 2003 *Phys. Plasmas* **10** 1443
- [12] Zhu W. et al 2006 *Phys. Rev. Lett.* **96** 225002
- [13] Shaing K.C., Cahyna P., Becoulet M., Park J.-K., Sabbagh S.A. and Chu M.S. 2008 *Phys. Plasmas* **15** 082506
- [14] Park J.-K., Boozer A.H. and Menard J.E. 2009 *Phys. Rev. Lett.* **102** 065002

- [15] Cole A.J., Callen J.D., Solomon W.M., Garofalo A.M., Hegna C.C., Lanctot M.J., Reimerdes H. and the DIII-D Team 2011 *Phys. Plasmas* **18** 055711
- [16] Kim K., Park J.-K., Kramer G.J. and Boozer A.H. 2012 *Phys. Plasmas* **19** 082503
- [17] Sasinowski M. and Boozer A.H. 1997 *Phys. Plasmas* **4** 3509
- [18] White R.B. 1990 *Phys. Fluids B* **2** 845
- [19] Williams J.D. and Boozer A.H. 2003 *Phys. Plasmas* **10** 103
- [20] Satake S., Park J.-K., Sugama H. and Kanno R. 2011 *Phys. Rev. Lett.* **107** 055001
- [21] Kim K., Park J.-K. and Boozer A.H. 2013 *Phys. Rev. Lett.* **110** 185004
- [22] Shaing K.C., Sabbagh S.A. and Chu M.S. 2009 *Plasma Phys. Control. Fusion* **51** 035009
- [23] Logan N.C., Park J.-K., Kim K., Wang Z. and Berkery J.W. 2013 *Phys. Plasmas* **20** 122507
- [24] Shaing K.C., Sabbagh S.A. and Chu M.S. 2010 *Nucl. Fusion* **50** 025022
- [25] Linsker R. and Boozer A.H. 1982 *Phys. Fluids* **25** 143
- [26] Mynick H.E. 1986 *Nucl. Fusion* **26** 491
- [27] Park J.-K. *et al* 2013 *Phys. Rev. Lett.* **111** 095002
- [28] Cole A.J., Hegna C.C. and Callen J.D. 2008 *Phys. Plasmas* **15** 056102
- [29] Bécoulet M. *et al* 2009 *Nucl. Fusion* **49** 085011
- [30] Schaffer M.J. *et al* 2011 *Nucl. Fusion* **51** 103028
- [31] Satake S., Sugama H., Kanno R. and Park J.-K. 2011 *Plasma Phys. Control. Fusion* **53** 054018
- [32] Park J.-K., Boozer A.H. and Glasser A.H. 2007 *Phys. Plasmas* **14** 052110
- [33] Burrell K.H., Garofalo A.M., Solomon W.M., Fenstermacher M.E., Osborne T.H., Park J.-K., Schaffer M.J. and Snyder P.B. 2012 *Phys. Plasmas* **19** 056117
- [34] Park J.-K., Boozer A.H., Menard J.E., Garofalo A.M., Schaffer M.J., Hawryluk R.J., Kaye S.M., Gerhardt S.P., Sabbagh S.A. and the NSTX Team 2009 *Phys. Plasmas* **16** 056115
- [35] Garofalo A.M. *et al* 2011 *Nucl. Fusion* **51** 083018
- [36] Sun Y. *et al* 2012 *Nucl. Fusion* **52** 083007
- [37] Satake S., Park J.-K., Sugama H. and Kanno R. 2013 *Nucl. Fusion* **53** 113033
- [38] Menard J.E. *et al* 2006 *Phys. Rev. Lett.* **97** 095002
- [39] Gerhardt S.P., Menard J.E., Park J.-K., Bell R., Gates D.A., Le Blanc B.P., Sabbagh S.A. and Yuh H. 2010 *Plasma Phys. Control. Fusion* **52** 104003